Elucidation of structure and dynamics in solid octafluoronaphthalene from combined NMR, diffraction and molecular dynamics studies

Andrew J. Ilott, Sebastian Palucha, Andrei S. Batsanov, Mark R. Wilson,* and Paul Hodgkinson*

Department of Chemistry, Durham University, South Road, Durham DH1 3LE, United Kingdom

E-mail: mark.wilson@durham.ac.uk; paul.hodgkinson@durham.ac.uk

Abstract

X-ray diffraction (XRD), molecular dynamics simulations (MD), and ^{19}F NMR have been used to investigate structure and dynamics in solid octafluoronaphthalene, $C_{10}F_8$. Two distinct processes are observed via measurements of ^{19}F relaxation times as a function of temperature; a faster process from T_1 relaxation with a correlation time of the order of ns at ambient temperature (fitting to Arrhenius-type parameters E_a = 20.6 $\pm$ 0.4 kJ mol^{-1} and $\tau_0 = 8 \pm 1 \times 10^{-14}$ s), and a much slower process from $T_{1\rho}$ relaxation with a correlation time of the order of μs (fitting to E_a = 55.1 $\pm$ 1.3 kJ mol^{-1} and $\tau_0 = 4 \pm 2 \times 10^{-16}$ s). Atomistic molecular dynamics reveals the faster process to involve a small angle jump of ~40° of the molecules, which is in perfect agreement with the X-ray diffraction study of the material at ambient temperature. The MD study reveals the existence of more extreme rotations of the molecules, which are proposed to enable the full rotation of the octafluoronaphthalene molecules. This explains both the $T_{1\rho}$ results and previous wideline ^{19}F NMR studies. The experimental measurements (NMR and XRD) and the MD computations are found to be strongly complementary and mu-

tally essential. The reasons why a process on the timescale of μs, and associated with such a large activation barrier, can be accessed via classical molecular dynamics simulations are also discussed.

Introduction

Octafluoronaphthalene, $C_{10}F_8$, has been regularly used as a model system for ^{19}F solid-state NMR, and yet key aspects of its structural chemistry have remained enigmatic, despite multiple NMR[1–3] and crystallographic[4–9] studies. The X-ray diffraction pattern of the room-temperature phase (I-OFN) reveals an unusually high level of thermal diffuse scattering and rapid fall of Bragg intensities with increasing Bragg angle,[4] indicating the presence of disorder; modeling this data with a single molecular orientation gave an unsatisfactory R-factor (35%).[5] Single-temperature diffraction data cannot determine whether this disorder is static or dynamic in nature, while variable temperature studies are hindered by complicated thermal polymorphism; on cooling below 266.5 K, I-OFN was reported to convert into a (poorly understood) phase with double unit cell volume (II-OFN, the reverse transition occurring at 281.8 K),[6,9] while we observed a different low-temperature phase (III-OFN).[7] This III-OFN phase has been determined by an independent X-ray study at 203 K,[8] although the phase transition was not explored.

The early ^{19}F NMR work had inferred the presence of dynamics in the ambient temperature phase of octafluoronaphthalene from a significant drop in the width of its wideline (static sample) ^{19}F spectrum as the sample was warmed between ca. 230 and 285 K.[1] This change occurred in roughly the same temperature range as the above-mentioned polymorphic transformations, and was interpreted as a transition from rigid structure to diffusional rotation around the C_2 axis perpendicular to the molecular plane (on the basis of symmetry information from the ^{19}F chemical shift anisotropy tensor, and by analogy with similar observations in hexafluorobenzene). However, the exact nature of the molecular motion remained unclear, as the full (180°) rotation seemed neither physically reasonable nor able to explain the diffraction results (since this rotation exchanges

crystallographically equivalent positions).

In this study, we have redetermined the crystal structure[10] and used NMR experiments and molecular dynamics simulations to resolve this puzzling collection of results. NMR obserables, such as relaxation times, are powerful probes of dynamic processes in the solid state,[11–14] particularly as different observables probe motional processes on different timescales. Spin-lattice relaxation, T_1, for example is sensitive to dynamics on the timescale of the NMR frequencies (typically hundreds of MHz) while spin-lattice relaxation in the rotating frame, $T_{1\rho}$, is sensitive to dynamics on the order of NMR nutation frequencies[15,16] (typically tens of kHz). As shown below, we observe strong temperature dependencies in both ^{19}F T_1 and ^{19}F $T_{1\rho}$ relaxation. Since these variations occur over a similar temperature range the same dynamic behavior cannot explain both sets of results, and the NMR measurements themselves cannot suggest the physical model required for their interpretation. From the data above, it is only possible to infer that the disorder observed in the diffraction studies is dynamic in nature.

The molecular dynamics simulations described below allow us to understand the disorder in I-OFN, and to rationalise the previously unexplained NMR results. MD provides a quantitative understanding of the faster process, for which a high degree of sampling was achieved not only because of the fast timescale of this process (of the order of nanoseconds) but also because the instrinsic symmetry of the crystalline state provides many equivalent molecules from which to sample. This also explains how a much slower process (with a timescale of a few microseconds) could also be observed, despite it being outside the range of classical atomistic MD simulations. This allows a plausible mechanism for the previously proposed C_2 rotation, and a full explanation of the NMR observations. MD simulations have been widely used to model relatively fast dynamics of proteins in solution[17] and to a lesser extent fast dynamic processes in molecular solids,[18–20] where the correlation times of the processes are comfortably within the simulation timescales of 10s of nanoseconds that are accessible to conventional atomistic MD. Similarly molecular mechanics (in conjunction with diffraction studies) has been used to rationalise experimental NMR results in solid systems exhibiting relatively free rotations.[21,22] Such simulations have not, however, pre-

viously been used to identify the slower processes that can be observed in NMR on the frequency scale of 10s of kHz via measurements of $T_{1\rho}$ relaxation or interference with magic-angle sample spinning.

Experimental: XRD and NMR

Single-crystal X-ray diffraction experiments were carried out on a Bruker SMART 1000 CCD area detector diffractometer, using graphite-monochromated Mo-Kα radiation ($\overline{\lambda} = 0.71073$ Å) and a Cryostream (Oxford Cryosystems) open-flow N_2 gas cryostat. The crystals were sealed in Lindemann capillaries to prevent sublimation. The computations used SHELXTL 6.14 software.[23]

A Varian UnityPlus spectrometer operating at a frequency of 282.2 MHz for ^{19}F was used for the measurements of the ^{19}F T_1 and $T_{1\rho}$ time constants. Octafluoronaphthalene was purchased from Alfa Aesar and samples packed into 4 mm o.d. magic-angle spinning (MAS) rotors. Although commercial samples typically contain small quantities of chlorinated source materials, these are at too low a level to influence the NMR measurements. (This was confirmed by test measurements on high purity samples obtained by vacuum sublimation.) T_1 time constants were measured using the saturation recovery pulse sequence.[24] $T_{1\rho}$ time constants were measured from the decay of spin-locked ^{19}F magnetisation using a ^{19}F RF nutation frequency of 83.3 kHz during the spin-lock period. The width of the ^{19}F spectrum makes it difficult to maintain an effective spin-lock over the full spectral width, and so these experiments were performed on static (non-spinning) samples, and the decay rate measured for the central portion of the spectrum where off-resonance effects are negligible. The measurements of T_1 are much less sensitive to off-resonance effects and so some data sets were also acquired under magic-angle spinning using an MAS rate of 8 kHz. The relaxation times were measured between –15 and 50 °C in increments of 5 °C. Below about –15 °C transformations into other forms occur (as discussed below) and results in this range were poorly reproducible. Both sets of relaxation data fitted well to single exponential curves, and fractional errors estimated from the fitting residuals were typically < 0.5 %.

MD simulations

Atomistic molecular dynamics simulations were performed on two systems of 144 octafluoronaphthalene molecules using periodic boundary conditions in each dimension. The first system corresponded to the high temperature phase (I-OFN), with the initial atomic positions taken from the atomic coordinates given by the XRD study described in this work. The repetition of the crystallographic unit cell to create the simulation block corresponds to an initial configuration with ordered "stacks" of molecules, in which half the stacks adopted one of the two "orientations" and half the alternate orientation. However, as discussed below, the orientations of the molecules quickly randomise during the simulation, which was carried out at 290 K. The second simulation system corresponded to III-OFN, with the starting configuration again derived from the XRD studies, and was run at two temperatures, 100 K (at which the phase is stable), but also at 290 K (where it is not stable).

The OPLS AA force field[25] was used as a starting point to model the intramolecular interactions. To optimize the generic force field for the system under study, the parameters for the non-bonded interactions obtained by Borodin *et al.*[26] from fits to results from *ab initio*studies were used. The partial atomic charges were also optimized; the electrostatic potential was calculated using the Gaussian 03 package[27] with the B972[28] model and the 6-311 G basis set, and fixed partial atomic charges were then fitted to this potential using the CHELPG scheme.[29] This allowed the simulations to better match the experimentally determined densities (2 % difference compared to 5 % using the default OPLS-AA parameters). The optimized parameters are given in the Supporting Information.

The simulations were run using DL_POLY 2.18.[30] Long range electrostatics were calculated using the Ewald sum method using a short-range cutoff of 1.2 nm. The system was equilibrated for 0.5 ns to the correct temperature, followed by a further 1.0 ns equilibration with unconstrained bond lengths. The bond lengths were then constrained using the SHAKE algorithm.[31] The simulations used the Nose Hoover algorithm[32] to run at constant pressure and temperature, using a 2 fs timestep. Atomic trajectories were sampled every 2 ps over 100 ns in the case of the high

temperature phase. The low temperature simulation was not expected to show interesting dynamic behavior and so a shorter production run of 8 ns was used.

Analysis

X-ray diffraction

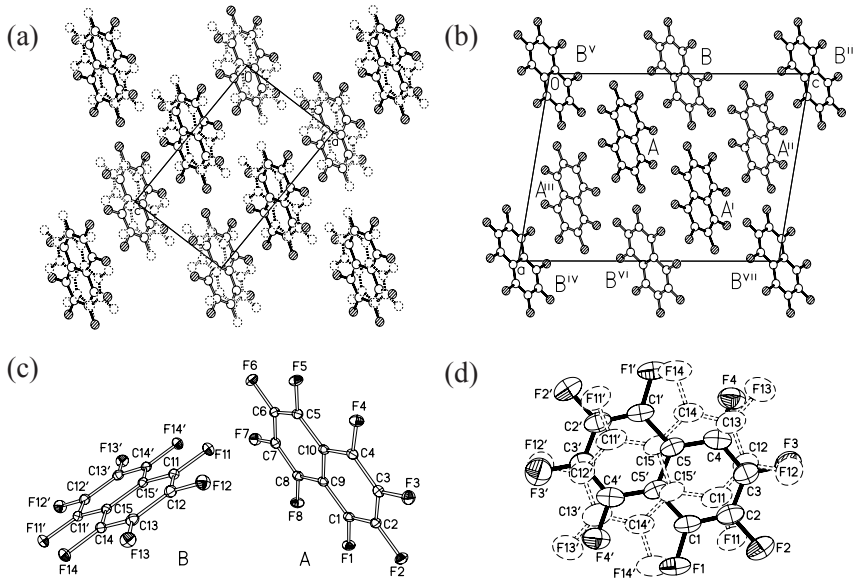

Figure 1: Crystal packing of (a) I-OFN and (b) III-OFN; (c) the two independent molecules, A and B, of III-OFN, (d) illustration of the molecular disorder in I-OFN. Thermal ellipsoids are drawn at the 50% probability level. Primed atoms are those generated by inversion centres.

The crystal structure of I-OFN was (re)determined at 290 K, with single crystals obtained by slow sublimation under static vacuum at room temperature, which gave much better diffraction than the specimens grown from solution. As shown in Figure 1(d), the molecular disorder was rationalized as two alternative orientations of the molecule, both centered at the same crystallographic inversion centre, co-planar within 1° but differing by a ca. 38° rotation around the molecular C_2 axis. Our results essentially agree with those of Gavezzotti *et al.*[33] although the better crystal quality allowed all atoms to be refined in anisotropic approximation and gave a much improved *R*-factor (3.1% vs 11.6%). The relative occupancies of the two orientations were refined,

converging at 54.2(7) and 45.8(7)%.

At 250±10 K the change of diffraction pattern indicated a phase transition which can be described by the (1, 0, 1; 0, −1 0; 2, 0, −1) transformation of the I-OFN lattice with a trebling of the unit cell volume, Figure 1(a & b). The transition was fully reversible in the selected crystallite, even after several cycles of cooling/warming. The lattice remained the same (apart from general contraction) from 240 K to 100 K, at which point the low-temperature structure was determined. This was in good agreementwith the previously published structure for III-OFN at 203 K.[8] The asymmetric unit comprises one molecule (A) in a general position and half of another molecule (B), located at a crystallographic inversion centre. If molecule B is shifted by the subcell translation (a/3, 0, c/3), its mean plane would coincide (within 0.1 Å, or 1°) with that of a symmetrical equivalent of A, A^{ii}, the orientations of the two molecules differing by a 38° rotation around their common centroid. The overlap is very similar to the disorder mode in phase I. The structure contains two symmetrically unrelated kinds of stacks, one formed only of molecules A and the other of molecules B. III-OFN has a subcell identical with the cell of I-OFN (Figure 1(a) and (b)) and can be regarded[33] as a modulated I-OFN. The packing in both forms is of the γ type[34] where both π-π (stacking) and π-σ interactions are important. Further details on the symmetry relations between the two phases can be found in the Supporting Information.

NMR

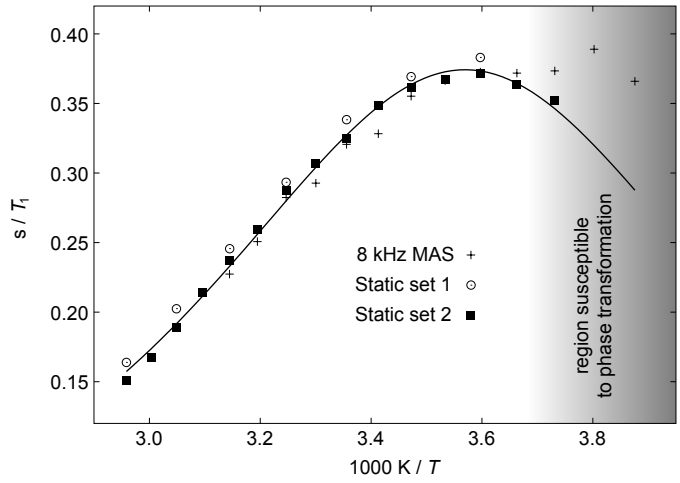

Figure 2: Compiled results from three sets of variable temperature T_1 measurements on octafluoronaphthalene. Error bars on the individual data points from the exponential fitting are of the order of the size of the symbols. The curve is a fit of the filled square data points to Eq. 3.

Figure 2 shows the variation of the ^{19}F spin-lattice relaxation time constant with temperature. Above the onset of the phase transition (about –15 °C or 1000 K / $T \approx 3.8$) the results are highly reproducible and show a classic form with maximum relaxation rate at about 1000 K / $T \approx 3.6$, where the motional process must be of the order of the ^{19}F NMR frequency ν_0 (here 282 MHz).

The spin-lattice relaxation is driven by motions that modulate the NMR frequency, via changes in NMR parameters such as the chemical shift anistropy (CSA) or dipolar couplings. A given mechanism contributes terms of the form

$$R_1 = A_1 J(\nu_0) + A_2 J(2\nu_0) \tag{1}$$

to the overall relaxation rate, where A_1 and A_2 are constants which depend on the relaxation mechanism and the NMR parameters involved, and $J(\nu)$ is the spectral density of the motion at a given

frequency. $J(\nu)$ is effectively the Fourier transform of a correlation function describing the time modulation of the relevant NMR interactions. For simple processes where the correlation function is a decaying exponential with a single characteristic correlation time, τ, the spectral density has the form,

$$J(\nu) = \frac{2\tau}{1+(2\pi\tau\nu)^2} \tag{2}$$

Although this spectral density is widely used for isotropic diffusion processes in the liquid state, it is also applicable to the restricted jump processes that are typical in crystalline solids. More complex spectral density functions are required in less ordered materials where distributions of local environments are present.[35]

The overall relaxation rate will contain terms involving the spectral density at ν_0 and $2\nu_0$. However, the complexity of relaxation processes in the solid-state generally precludes analytical prediction of the overall A_1 and A_2 coefficients, and the difference between the $J(\nu_0)$ and $J(2\nu_0)$ functions is too subtle to allow the coefficients to be fitted independently. Hence further analysis uses a single spectral density at ν_0.

If we assume that the kinetics follow Arrhenius behaviour then $\tau = \tau_0 \exp(E_a/RT)$, and the data should fit to

$$\frac{1}{T_1} \propto \frac{\tau_0 \exp\left(\frac{E_a}{RT}\right)}{1+(2\pi\tau_0\nu_0)^2 \exp\left(\frac{2E_a}{RT}\right)} \tag{3}$$

providing τ_0 and the activation barrier, E_a. Note that the simplification to a single spectral density has no effect on the derived E_a. The fit shown in Figure 2 gave an E_a of 20.6 $\pm$ 0.4 kJ mol^{-1}, and a τ_0 of $8 \pm 1 \times 10^{-14}$ s. As shown below, this motional process is likely to correspond to the dynamic disordering of the octafluoronaphthalene molecules.

Figure 3 shows the corresponding plot for the measurements of $T_{1\rho}$. Although $T_{1\rho}$ values can be affected by processes other than dynamics (such as "spin diffusion"), these processes will be largely temperature independent and cannot explain the strong variation observed in Figure 3. The same analysis as above can then, in principle, be used to extract the kinetic parameters for the

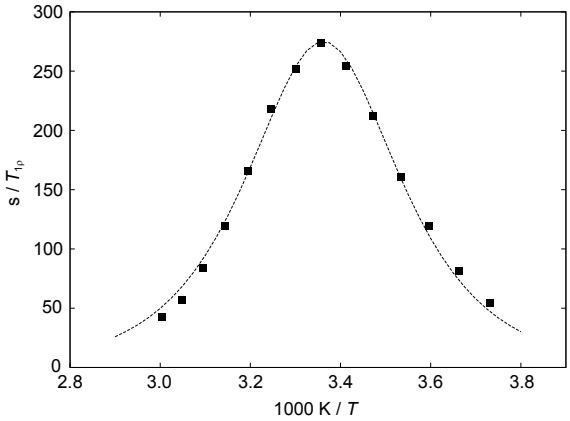

Figure 3: Results from variable temperature $T_{1\rho}$ measurements, together with the fit used to extract the kinetic parameters. Error bars on the individual data points are of the order of the size of the symbols used.

slower motional process, except the relevant frequency is the RF nutation frequency $\nu_1 = 83.3$ kHz. This gives an activation barrier of 55.1 $\pm$ 1.3 kJ mol^{-1} and time constant, τ_0 of $4 \pm 2 \times 10^{-16}$ s. As expected, this slower motion corresponds to a higher energy process than that observed in T_1. However, it is not possible to determine the nature of the dynamic process directly from the NMR results.

Molecular dynamics

The rigid nature of the octafluoronaphthalene molecules and their confinement within a well-defined crystalline structure mean that the key degrees of freedom are those describing the molecular orientation. As shown in Figure 4, the molecular orientation is defined with respect to a fixed molecular frame, whose $\vec{x}$ and $\vec{y}$ axes are determined by the vectors pointing between the fluorine atoms, with the $\vec{z}$-axis given by the cross product of $\vec{x}$ and $\vec{y}$. This molecular frame allows the relative orientations of different molecules in the simulation cell to be compared, and an ensemble average over all of the molecules to be taken. To follow the evolution of the molecular orientations

over the course of the simulation, a common reference frame ($\vec{x}_0$, $\vec{y}_0$, $\vec{z}_0$) was defined using the average orientation of the molecules in the first simulation step after equilibration. At each time step, projections of $\vec{y}$ and $\vec{z}$ and for each molecule on to the $\vec{x}_0\vec{y}_0$ and $\vec{y}_0\vec{z}_0$ planes were used to define the vectors $\vec{y}_p$ and $\vec{z}_p$ respectively. The angles between these projections and the reference frame defined the orientation in spherical polar coordinates, with the angle between $\vec{y}_p$ and $\vec{y}_0$ giving ϕ and the angle between $\vec{z}_p$ and $\vec{z}_0$ giving θ.

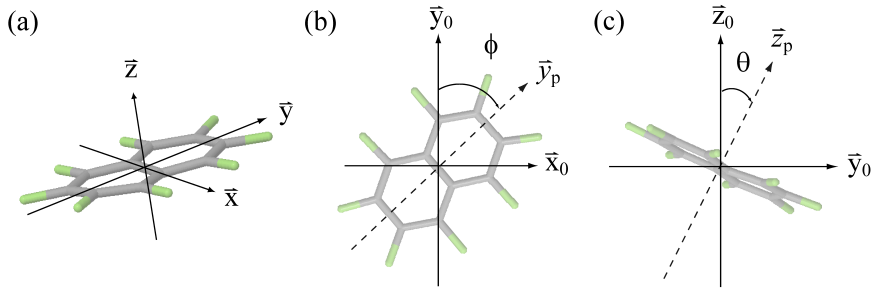

Figure 4: Illustration of the molecular frame used to define the orientation of each octafluoronaphthalene molecule in the simulation. (a) The three orthogonal axes are defined in terms of the atomic positions in the molecule, and the orientation of the molecule at a given instant defined using the orientation of this frame relative to the average starting positions ($\vec{x}_0$, $\vec{y}_0$, $\vec{z}_0$) of all the molecules in the simulation (b and c).

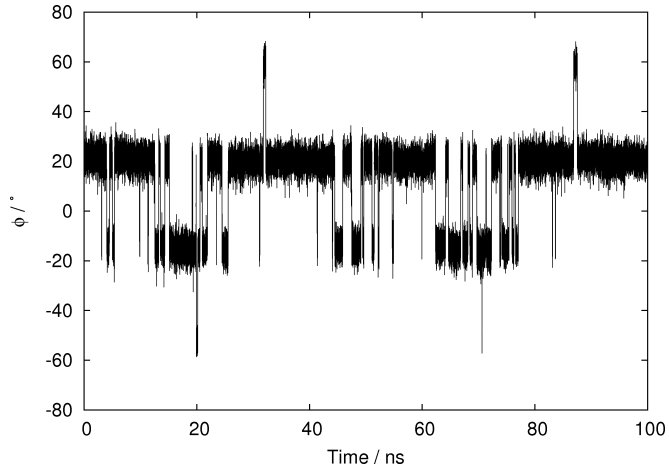

Figure 5: Time evolution of the ϕ polar angle for a selected octafluoronaphthalene molecule during the course of the 290 K simulation, showing jumps between four distinct orientations.

Figure 5 shows the evolution of the ϕ polar angle during the course of the 290 K simulation for one selected octafluoronaphthalene molecule. Most of the time is spent in two positions, related by a rotation of the molecule of approximately 40°, which is consistent with the modeling of the X-ray diffraction data. The relative occupancy of these two sites is not exactly equal and is a good match for the small, but statistically significant inequivalence observed by X-ray crystallography noted above. The molecule also infrequently occupies another two orientations, which correspond to a jump of a further $\approx$40° away from the two principal orientations. These orientations are illustrated in Figure 6(b), but are so rarely occupied that they would have negligible effect on the Bragg scattering and would not be detected in the XRD studies.

The frequencies of occupancy of the different orientations of all the molecules in the simulation cell were combined and used to estimate the relative potential energy of the molecules as a function of their orientation within the crystal structure. Figure 6(a) shows that the different orientations can be largely defined in terms of ϕ (i.e. rotation perpendicular to the molecular plane), but that there is also a slight wobble of the molecular plane. Figure 6 (b) shows a cross section through the two dimensional energy surface through a path passing through all the energy minima. The lower energy barrier around $\phi = 0°$ is quite well defined and can be estimated at $\approx$14 kJ mol^{-1} with a rate, *k*, at 290 K of approximately 0.56 ns^{-1}. This corresponds to a correlation time $\tau = 1/2k = 0.89$ ns, which compares well with a value of 0.4 ns at 290 K predicted from the Arrhenius parameters derived from the NMR study. In contrast, the high energy orientations are sampled less well, even with this simulation run of 100 ns, precluding accurate estimation for the energy barrier for accessing these sites. However, the simulations do allow us to deduce a lower limit of 27 kJ mol^{-1}.

At first glance, it is surprising that we can access such high energy states at all using conventional atomistic molecular dynamics simulations; we would normally argue that simulations running over tens of ns cannot (and should not) be used to probe microsecond timescale dynamics. However, the equivalence of the sites due to the crystalline symmetry, combined with the rigid nature of the individual molecules, means that it is legitimate to take ensemble averages over all of the 144 molecules of the simulation box and consider this as a single molecular trajectory. In

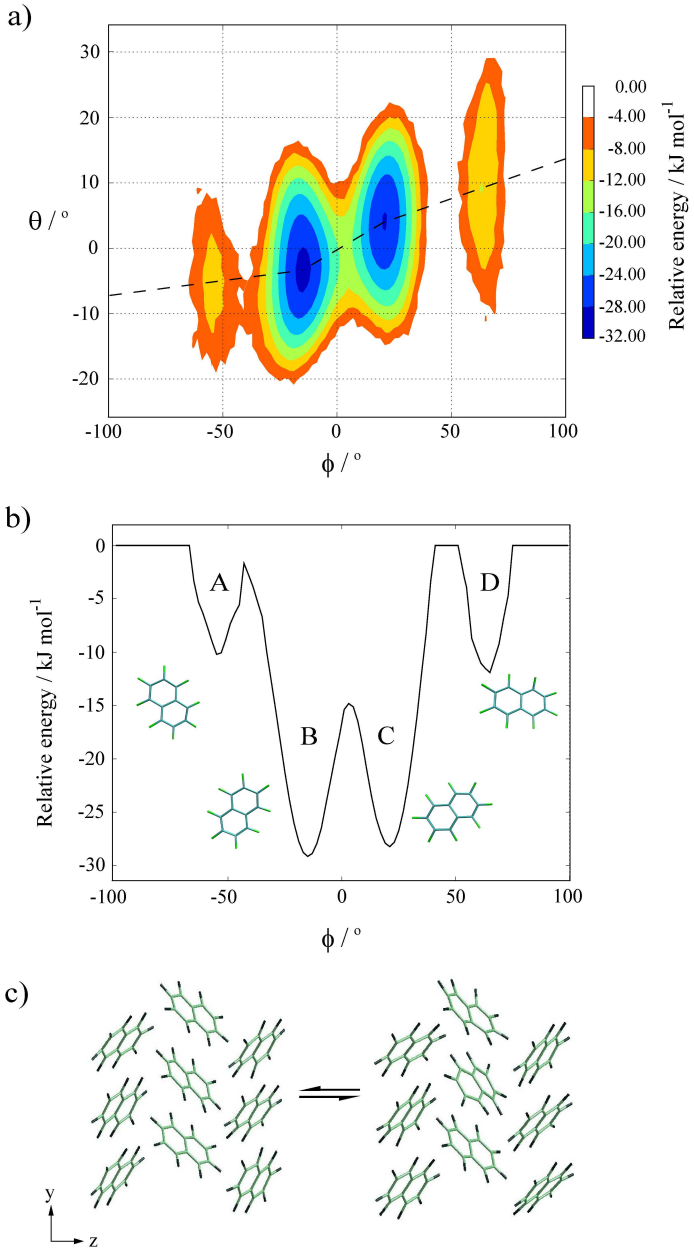

Figure 6: (a) Potential energy surface of octafluoronaphthalene as a function of molecular orientation, defined in terms of the polar angles ϕ and θ. The relative energies are calculated from the Boltzmann distributions of the different states combined over all the time steps and all the molecules in the simulation (with histogram bin widths of 2°). (b) Slice through the lowest energy pathway between the four stable positions, indicated by the dashed line. (c) An example of a molecule reorienting within its local crystal structure; the molecule at the centre of the figure is seen to rotate by approximately 40°.

effect, we can observe the dynamics of a single molecule over 14.4 μs. Clearly this "timescale multiplication" is only valid when considering, say, molecular orientations, and is not applicable to other features of the dynamics, such as the correlations between the orientations of neighboring molecules.

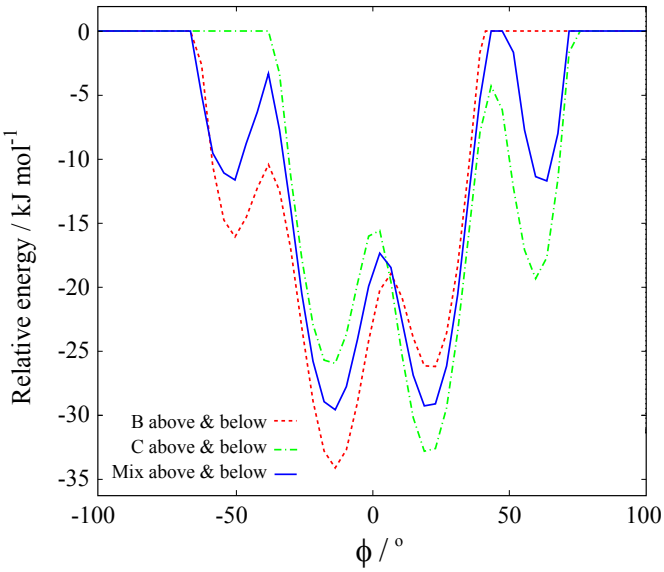

Figure 7: Pseudo-potential for octafluoronaphthalene orientation as Figure 6, but determined from statistics collected separately for different combinations of neighboring group orientation.

That such correlations exist can be demonstrated by collecting statistics separately depending on the orientation of the neighboring molecules in the octafluoronaphthalene stacks. Figure Figure 7 shows the resulting effective potential experienced by a molecule depending on the orientations of its neighbors, and shows that it is significantly more favorable for a molecule to adopt the same (major) orientation as its neighbors. Although the level of sampling is much poorer, simulations at artificially high temperatures (390 K, above the sublimation point) showed that all four orientations are still accessible for any given molecule, i.e. the dynamics are modified, but not fundamentally changed by the effects of correlation. It is important to bear in mind that the periodic boundary conditions may interact with the length scale / periodicity of the correlation. But

since the modification to the energies even for the nearest neighbors is quite small (approximately ± 4 kJ mol^{-1}), the effects of the periodic boundary conditions are expected to be negligible. The effects of short-range correlation have not been analysed in further detail since they are not readily linked to the experimental measurements which probe ensemble averages.

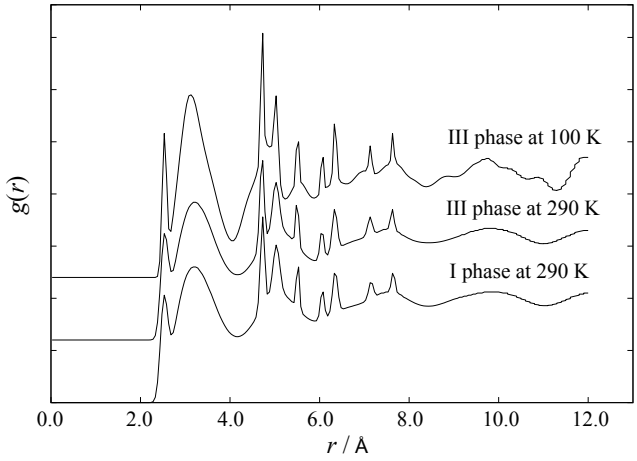

Figure 8: Fluorine radial distribution functions derived from simulations of I-OFN at 290 K, and III-OFN at both 100 K and 290 K. The *g(r)* for the form III simulations are vertically shifted for clarity.

The simulations also clarify the relationship between the I and III phases. Figure 8 compares the overall radial distribution functions, *g(r)*, between all the fluorine atoms for the three simulations. This is a convenient means of comparing the different structures, particularly as the unit cells of the I and III phases are not trivially related, meaning that the atomic coordinates from the simulation boxes cannot be simply overlaid. The three functions share the same basic structure, confirming that the crystal structures are very similar. The lower symmetry, low temperature structure has, as expected, a slightly more structured distribution function, particularly at longer distance. However, on warming this phase, the $g(r)$ changes, most notably at around r = 3.5 Å and above 8 Å, and becomes indistinguishable from that of Form I. It is also worth noting that the stacks of III-OFN are orientationally ordered. Figure 7 shows that ordering neighboring ori-

entations is favorable even in I-OFN, suggesting that the transformation to III-OFN involves the freezing in of orientational order along the stacks.

Discussion

The identification of the fast process observed in the molecular dynamics simulations with the process reponsible for the temperature dependence of T_1 is straightforward, since both timescales and estimated barriers are in agreement. An exact match between the E_a of 20.6 $\pm$ 0.4 kJ mol^{-1} obtained from NMR and the $\Delta G^{\ddagger}$ at 290 K of $\approx$14 kJ mol^{-1} estimated from the MD is not expected, partly because E_a and $\Delta G^{\ddagger}$ are not strictly comparable, and partly due to instrinsic limitations of MD simulations; the estimated energy barrier will be very sensitive to the exact parameterisation of the force field. These results are also in excellent agreement with the model used to fit the X-ray diffraction data, with the NMR and MD confirming that the disorder is dynamic in nature.

The motion observed in $T_{1\rho}$ is more interesting as both NMR and Molecular Dynamics are required to understand the experimental observations. At first sight, the presence of a process on a μs timescale in Figure 5 provides a simple explanation for the observed temperature dependence of $T_{1\rho}$. However, this is not supported by relaxation theory. Considering the simplest model which involves a rarely occupied site of exchange between inequivalent sites A and B, the expression for the relaxation rate will be of the form:[36]

$$\frac{1}{T_1} \propto p_A(1-p_A)(A_1 J(\nu) + A_2 J(2\nu)) \tag{4}$$

where p_A is the fractional occupancy of state A, ν is the relevant frequency (here the RF nutation frequency) and $A_{1,2}$ are coefficients that depend on NMR parameters and geometrical factors. The correlation time in the spectral density functions (cf. Eq. 2) is given by $\tau = (k_{AB} + k_{BA})^{-1}$, where k_{AB} and k_{BA} are jump rates from state A to B and B to A respectively. This, together with the relaxation rate, is dominated by the faster process. The temperature dependence of the relaxation rate is also determined by the lower of the two activation barriers. Including all four orientations

(A–D in Figure 6) does not fundamentally change this picture. It could be argued that classic relaxation theory is inappropriate for $T_{1\rho}$ since the RF nutation frequency is not very much larger than the modulation of the NMR frequency due to the dynamics. Exact quantitative modelling of $T_{1\rho}$ requires an analysis which puts the Hamiltonian terms, including the RF, on the same footing as the exchange. We have previously used such an approach to show how the interaction between exchange processes and RF irradiation results in magnetisation decay which is equivalent to $T_{1\rho}$ in classic relaxation theory.[37] However, numerical simulations confirm that the decay rates are still dominated by the faster processes, and the presence of a slow relaxation rate cannot be explained by the four site model derived from Figure 6.

As discussed in the introduction, early NMR work[1] had suggested that the octafluoronaphthalene molecules might undergo 180° jumps about an axis perpendicular to the molecular plane. Such a rotation appears physically unrealistic, particularly when other motions e.g. jumps about the long molecular axis would be expected to involve lower energy barriers. The MD results, however, provide a plausible mechanism for such a rotation, via the rarely occupied sites. Recognising that there are corresponding set of four orientations related by inversion symmetry (say A'–D'), then only a further rotation of ~60° is required to take a molecule from one extreme orientation to another, A↔D' or A'↔D. As discussed in more detail in the Supporting Information, this eight site model *is consistent* with an overall 180° rotation occuring at a relatively slow rate, although the simulations reveal that the underlying molecular process involves intermediate steps. Note that the overall rotation of the molecules is never observed in the ambient temperature MD results, which is a consequence of the low probability for the jump between extreme orientations combined with the low occupancy of these states. However, running the simulations at an artificially high temperature of 390 K (well above the sublimation point) did result in a full rotation of the molecules, as predicted. The narrowing of the wideline NMR spectrum shows that a significant motion must be occurring that affects the entire sample (rather than being associated with defects). Similarly the temperature dependence of $T_{1\rho}$ is only consistent with a process on a μs timescale involving all molecules, rather than a subset.

This work highlights the complementary nature of the experimental work (NMR and XRD) and the MD simulations. The NMR provides robust measurements of kinetic parameters, in this case thermal activation barriers and correlation times, but is unable to identify the molecular motions associated with the NMR observables. Similarly the diffraction study was able to model the disorder associated with the fast process, but could not itself determine the nature of this disorder, or detect jumps preserving the crystallographic symmetry. Previous literature had argued for a single process involving a C_2 jump process in the molecular plane. However, this could not explain the temperature-dependence of both T_1 and $T_{1\rho}$ relaxation rates. The molecular dynamics simulations allow the T_1 relaxation to be straightforwardly linked with jumps of about 40° between two orientations. The equivalence of different molecules in the crystal means that we have also been able to observe a much rarer process occuring on a microsecond timescale, which would not normally be accessible to conventional atomistic MD. The C_2 jump process in the molecular plane deduced from earlier wideline NMR measurements is likely to occur via these states, but their low occupancy means that these states could not be identified from the experimental measurements. In contrast, molecular dynamics simulation relied on experimental characterisation of the crystal structure from diffraction experiments, and its estimates of kinetic parameters are strongly dependent on the force field used and its parameterisation. The experimental NMR measurements are considerably more robust, and capable of observing extremely rare processes that are beyond the range of atomistic MD.

In recent years, the search for tractable molecular machines[38,39] has increased interest in dynamics occurring in the solid state. Octafluoronaphthalene is not itself a good candidate for such systems because the jump processes and correlated motions are associated with large energy barriers. However, the work presented here does highlight the importance of considering even the slowest degrees of freedom, as they can lead to new phenomena that can fundamentally change the way a system behaves (cf. the small molecular jumps which provide the mechanism for the full rotation of the molecules). In particular, correlated motions are seen to modify the energy landscape explored by a system in a non-trivial way, and must be understood if the goal of creating

effective molecular machines is to be realized.[22,40] Molecular dynamics simulations are uniquely suited to looking at these effects, and are highly complementary to experimental NMR studies in probing complex motional processes.

Acknowledgments

Andrew J. Wilkinson is thanked for his early measurements of ^{19}F relaxation times. Samples purified by vacuum sublimations were provided by Jonathan C. Collings. Robin Harris (Durham) and Nikolai Skrynnikov (Purdue) are thanked for helpful discussions. SP was supported under EPSRC grant EP/D055237/1. AJI is supported through EPRSC's Doctoral Training Account scheme.

Supporting information available

The Supporting Information contains: force field parameters for the MD simulations, details of the X-ray crystallography and the associated structural analysis, crystallographic data for I-OFN and III-OFN (CCDC deposition numbers 757890 and 757891 respectively) and the complete reference 21. This information is available free of charge at http://pubs.acs.org.

References

(1) Mehring, M.; Griffin, R. G.; Waugh, J. S. *J. Chem. Phys.* **1971**, *55*, 746.

(2) Harris, R. K.; Jackson, P.; Nesbitt, G. J. *J. Magn. Reson.* **1989**, *85*, 294–302.

(3) Robbins, A. J.; Ng, W. T. K.; Jochym, D.; Keal, T. W.; Clark, S. J.; Tozer, D. J.; Hodgkinson, P. *Phys. Chem. Chem. Phys.* **2007**, *9*, 2389–96.

(4) Del Pra, A. *Acta Crystallogr. B* **1972**, *29*, 3433–9.

(5) Akhmed N. A., *Zh. Strukt. Khim.* **1973**, *14*, 573–574.

(6) Pawley, G. S.; Dietrich, O. W. *J. Phys. C* **1975**, *8*, 2549–2558.

(7) Collings, J. C.; Roscoe, K. P.; Thomas, R. L.; Batsanov, A. S.; Stimson, L. M.; Howard, J. A. K.; Marder, T. B. *New J. Chem.* **2001**, *25*, 1410–1417.

(8) Bagryanskaya, I. Y.; Gatilov, Y. V.; Lork, E.; Mews, R.; Shakirov, M. M.; Watson, P. G.; Zibarev, A. V. *J. Fluor. Chem.* **2002**, *116*, 149–156.

(9) Mackenzie, G. A.; Arthur, J. W.; Pawley, G. S. *J. Phys. C* **1977**, *10*, 1133–1149.

(10) While the present work was in progress, the disorder in I-OFN was interpreted [Cozzi 2007] in good agreement with our own results.

(11) Abragam, A. *Principles of Nuclear Magnetism*; Oxford Univ. Press, 1961.

(12) Tycko, R. How does NMR probe molecular dynamics? In *Nuclear Magnetic Resonance Probes of Molecular Dynamics*; Tycko, R., Ed.; Kluwer Academic Publishers, 1994; pp 1–26.

(13) Hodgkinson, P. In *NMR Crystallography*; Harris, R. K., Wasylishen, R. E., Duer, M. J., Eds.; EMR Handbooks; Wiley, 2009; Chapter Intramolecular motion in crystalline organic solids.

(14) Schmidt-Rohr, K.; Spiess, H. W. *Multidimensional Solid-State NMR and Polymers*; Academic Press, 1994.

(15) Hasebe, T.; Strange, J. H.; Nakamura, N.; Chihara, H. *J. Chem. Soc. Faraday Trans. 2* **1985**, *81*, 749–756.

(16) Riddell, F. G.; Arumugam, S.; Harris, K. D. M.; Rogerson, M.; Strange, J. H. *J. Am. Chem. Soc.* **1993**, *115*, 1881–1885.

(17) Case, D. A. *Acc. Chem. Res.* **2002**, *35*, 325.

(18) George, A. R.; Harris, K. D. M. *J. Mater. Chem.* **1994**, *4*, 1731.

(19) Vold, R. L.; Hoatson, G. L.; Subramian, R. *J. Chem. Phys.* **1998**, *108*, 7305–16.

(20) Albunia, A. R.; Gaeta, C.; Neri, P.; Grassi, A.; Milano, G. *J. Phys. Chem. B* **2006**, *110*, 19207.

(21) Khuong, T. A. V.; Dang, H.; Jarowski, P. D.; Maverick, E. F.; Garcia-Garibay, M. A. *J. Am. Chem. Soc.* **2007**, *129*, 839–845.

(22) Jarowski, P. D.; Houk, K. N.; Garcia-Garibay, M. A. *J. Am. Chem. Soc.* **2007**, *129*, 3110–3117.

(23) *SHELXTL, Version 6.14*, Bruker AXS, Madison, Wisconsin, USA, 2003.

(24) Markley, J. L.; Horsley, W. J.; Klein, M. P. *J. Chem. Phys.* **1971**, *55*, 3604–5.

(25) Jorgensen, W. L.; Maxwell, D. S.; Tirado-Rives, J. *J. Am. Chem. Soc.* **1996**, *118*, 11225–11236.

(26) Borodin, O.; Smtih, G. D.; Bedrov, D. *J. Phys. Chem. B* **2002**, *106*, 9912–9922.

(27) Frisch, M. J. et al. *Gaussian 03*, Gaussian Inc., Wallingford, CT, 2004.

(28) Wilson, P. J.; Bradley, T. J.; Tozer, D. J. *J. Phys. Chem. B* **2002**, *115*, 9233–9242.

(29) Breneman, C. M.; Wiberg, K. B. *J. Comput. Chem.* **1990**, *11*, 361–373.

(30) Smith, W.; Forester, T. *J. Mol. Graph.* **1996**, *14*, 136.

(31) Ryckaert, J. P.; Ciccotti, G.; Berendsen, H. J. C. *J. Comput. Phys.* **1977**, *23*, 327.

(32) Hoover, W. G. *Phys. Rev. A* **1985**, *31*, 1695–1697.

(33) Cozzi, F.; Bacchi, S.; Filippini, G.; Pilati, T.; Gavezzotti, A. *A. Chem. Eur.* **2007**, *13*, 7177–7184.

(34) Desiraju, X.; Gavezzotti, A. *Acta Crystallogr. B* **1989**, *45*, 473–482.

(35) Beckmann, P. A. *Phys. Rep.* **1988**, *171*, 85–128.

(36) Torchia, D. A.; Szabo, A. *J. Magn. Reson.* **1982**, *49*, 107–121.

(37) McMillan, D. E.; Hazendonk, P.; Hodgkinson, P. *J. Magn. Reson.* **2003**, *161*, 234–241.

(38) Khoung, T. A. V.; Nunez, J. E.; Godinez, C. E.; Garcia-Garibay, M. A. *Acc. Chem. Res.* **2006**, 413–422.

(39) Kay, E. R.; Leigh, D. A.; Zerbetto, F. *Angew. Chem. Int. Ed.* **2007**, *46*, 72–191.

(40) Ikeuchi, S.; Miyazaki, Y.; Takeda, S.; Akutagawa, T.; Nishihara, S.; Nakamura, T.; Saito, K. *J. Chem. Phys.* **2005**, *123*, 044514.